ACS OMEGA

Open Access

http://pubs.acs.org/journal/acsodf

Article

Green Synthesizing and Corrosion Inhibition Characteristics of Azo Compounds on Carbon Steel under Sweet Conditions: Experimental and Theoretical Approaches

Kamal Shalabi,* Hany M. Abd El-Lateef, Mohamed M. Hammouda, and Antar A. Abdelhamid

Cite This: *ACS Omega* 2024, 9, 18932−18945

Read Online

ACCESS | Metrics & More | Article Recommendations | Supporting Information

ABSTRACT: The deterioration of carbon steel in saline solutions enriched with carbon dioxide represents a significant challenge within the oil and gas industry. So, this study focuses on the design and structural analysis of four azo derivatives: 4-(2-quinolinylazo)-catechol (AZN-1), 4-(4-phenoxyphenylazo)-1-naphthol (AZN-2), 4-(4-pyridylazo)-1-naphthol (AZN-3), and 4-(2-pyridylazo)-1-naphthol (AZN-4), and their first application as effective corrosion inhibitors for carbon steel in a carbon dioxide saturated 3.5% sodium chloride solution. Spectroscopic methods were used to characterize the structural configurations of these compounds. The corrosion protection properties of these compounds on carbon steel in a carbon dioxide saturated 3.5% sodium chloride solution (under sweet conditions) were investigated using Tafel polarization (PDP), electrochemical impedance spectroscopy (EIS), and field emission-scanning electron microscopy (FE-SEM) studies. The results indicate that the inhibition efficiency increases as the concentration of the inhibitors increases. There is a notable agreement between the results obtained from the PDP and EIS measurements, supporting the findings. Moreover, the results displayed that these compounds had significant corrosion protection capabilities at low concentrations, ranging from 91.0 to 98.3% at an additive concentration of 5×10^{-4} M. The PDP profiles showed that these compounds acted as mixed inhibitors, and their adsorption behavior followed the Langmuir isotherm model. Besides, EIS results corroborate the adsorption of AZN compounds through a reduction in double-layer capacitance (C_{dl}) alongside an augmentation in polarization resistance (R_p) after the addition of AZN compounds into the corrosive solution. Field emission scanning electron microscopy (FE-SEM) and Fourier-transform infrared spectroscopy (FTIR) analysis confirmed the formation of a protective layer on the surface of carbon steel when these inhibitors were applied. In addition, computational calculations and Monte Carlo simulations were performed to support the experimental observations, gain insights into the adsorption properties, and elucidate the corrosion inhibition mechanisms of these compounds.

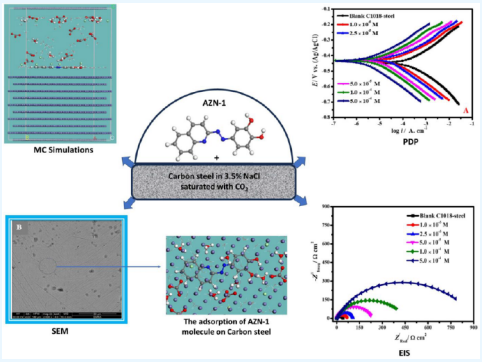

1. INTRODUCTION

Carbon steel is recognized for its excellent mechanical properties and is commonly used in the oil and gas industry for construction and transportation purposes.[1] Nevertheless, the pipelines utilized for the transport of crude oil may be subjected to various problems resulting from corrosion.[2] A particularly relevant challenge within the petroleum industry is corrosion attributable to carbon dioxide. Although carbon dioxide itself is not corrosive, its interaction with water results in the formation of carbonic acid, a compound of significant corrosiveness that has the potential to inflict substantial damage upon steel pipes.[3] So, corrosion inhibitors are widely utilized as a cost-effective and easily applicable method to mitigate corrosion. In the oil industry, inorganic inhibitors like arsenates and chromates are frequently employed to prevent corrosion.[4] However, these compounds pose environmental and biological risks. On the other hand, organic inhibitors[5] such as imidazoline,[6] pyrimidine,[7] thiadiazole,[8] phosphate,[9] and surfactants[10] are employed for CO_2 corrosion. These organic inhibitors have benzene rings and heteroatoms such as nitrogen, oxygen, phosphor, and sulfur, which absorb onto metal surfaces and reduce the corrosion.[11] Nevertheless, these organic inhibitors need to be applied in large quantities and can be harmful to the environment. As a result, research in corrosion inhibition has concentrated on the development of naturally friendly replacements known as "green corrosion inhibitors." Examples of these include plant extracts,[12,13] amino acid derivatives,[14] natural polymers,[15] and pharmaceuticals.[16]

Azo dye compounds are organic material behaviors that have Ar−N=N−Ar′ the functional group, where Ar and Ar′ are

Received: November 14, 2023
Revised: March 28, 2024
Accepted: April 4, 2024
Published: April 19, 2024

Table 1. Comparison between Corrosion Inhibition of Recent Azo Dye Derivative Inhibitors for Carbon Steel Corrosion and the Investigated Azo Dye Derivatives in This Study

inhibitors code	corrosive medium	optimal concentration	maximum inhibition%	references
8		1×10^{-3} M	90.0	20
S1H	1 M HCl	5×10^{-3} M	91.0	27
acetyl B		7.50×10^{-4} M	96.1	28
SDCAC		1×10^{-4} M	98.6	29
S2		100 ppm	92.4	30
C2		6×10^{-5} M	87.3	31
CMBTAP		20×10^{-5} M	67.7	32
5a	2.0 M HCl	21 $x10^{-6}$ M	92.1	33
Pz1	15% M HCl	2000 ppm	91.0	34
AS	1.0 M H_2SO_4	8×10^{-5} M	91.3	35
[$NiLCl_2$]		400 ppm	92.3	36
AZN-1	3.5% NaCl statured with CO_2	5×10^{-4} M	98.3	this work
AZN-4			91.0	

usually aromatic rings. They are commercially significant compounds of azo products; azo dye components comprise more than 65% of all dye compounds employed in nutrition and material production.[17] Azo dye products are extensively employed to treat cloths, flogging articles, and some food products. Azo dye compounds currently represent the largest manufacturing volume in the dye industry, and their reputation is expected to increase further in the future. They play a significant role in the regulation and management of the dyes and printing market.[18] Azo dye compounds are synthesized using an easy process known as diazotization and coupling. Through various routes and modifications, the desired color properties, yield, and particle size of the dyes are achieved, resulting in improved dispensability.[19]

Azo dye compounds are the greatest significant designing colorants, which have been extensively employed in fabric, clothes, printing, industrial papers, corrosion inhibitors, etc.[20,21] Most azo dye compounds are prepared by diazotization of $ArNH_2$, followed by coupling with electron-rich nucleophile compounds like NH_2 and OH.[22] There are other procedures for designing the azo dye compounds[23] among these are reduction of nitroaryl compounds in basic solution, reduction of nitroso products via Li[AlH_4], oxidation of primary amine compounds using $KMnO_4$ or $Pb(C_2H_3O_2)_4$, condensation of hydrazine and quinone compounds, and condensation of Ar-NH_2 compounds with nitroso compounds. In addition, azo dyes that contain heterocyclic components demonstrate improved coloring characteristics, tinctorial strength, and thermal permanency and exhibit supplementary pronounced solvatochromic performance compared to dye components derivative from a basic $ArNH_2$. These attributes make them valuable contributors to the field of pharmaceuticals and drug development.[24,25]

The existence of nitrogen atoms within the azo linkage, in conjunction with the versatility afforded by the selection of substituent groups in the structure of the azo dyes, facilitates the design of molecules to meet the structural criteria necessary for organic corrosion inhibitors that reveal easy and robust adsorption onto the surface of steel.[26] Recent research findings indicate that in the past few years, azo dye derivatives have been increasingly employed as corrosion inhibitors for steel in acidic environments[20,27−36] (Table 1). Azo compounds are very easy for preparation, all starting materials for the synthesis of azo compounds are available and are cheaper, there is no loss of energy in the preparation, the reaction needs only cooling during the synthesis of azo dyes, and the yield of preparation is very high. It is worth noting that the application of azo dye derivatives as corrosion inhibitors in oilfield-produced water under acidic conditions is limited as delineated in Table 1. Hence, the main goal of this study is synthesizing and characterizing four azo dye derivatives (namely 4-(2-quinolinylazo)-catechol [AZN-1], 4-(4-phenoxyphenylazo)-1-naphthol [AZN-2], 4-(4-pyridylazo)-1-naphthol [AZN-3], and 4-(2- pyridylazo)-1-naphthol [AZN-4]) and their first use as potential anticorrosion agents for carbon steel in a 3.5% sodium chloride solution saturated with carbon dioxide (under sweet conditions). The selection of AZN compounds as corrosion inhibitors is predicated on several factors: (i) they can be easily synthesized with lower cost; (ii) they possess numerous active sites with electron donation abilities; (iii) they exhibit a pronounced ability to mitigate the sweet corrosion of carbon steel, with efficacy ranging from 91.0 to 98.3%; (iv) they demonstrate robust adsorption on the carbon steel surface at 50 °C. The evaluation will be conducted using PDP, EIS measurements, surface examination analysis (FE-SEM and FTIR investigations), and additional confirmation through DFT calculations and MC simulations.

2. MATERIALS AND METHODS

2.1. Materials and Reagents. The purity of the chemical compounds employed was appropriate for use as analytical components (AR). These involved 4-(2-quinolinylazo)-catechol (AZN-1), 4-(4-phenoxyphenylazo)-1-naphthol (AZN-2), 4-(4-pyridylazo)-1-naphthol (AZN-3), and 4-(2- pyridylazo)-1-naphthol (AZN-4), in addition to organic solvent compounds, such as ethyl alcohol.

For electrochemical experiments, carbon steel grade 080A15 with an area of 4.55 cm^2 was utilized. The chemical composition of the steel, expressed in weight percent (wt %), is as follows: nickel (0.013), carbon (0.072), chromium (0.04), manganese (0.16), magnesium (0.28), silicon (0.029), and iron (remaining). To obtain a mirror polish on the surface of the C-steel alloy, it was abraded by using emery paper ranging from grades 600 to 2000. Subsequently, the surface was washed with bidistilled water and degreased using acetone.

2.2. Synthesis of (AZN) as the Azo Derivatives. *2.2.1. Step I: Synthesis of Diazonium Salt Azo Compounds.* A cooled mixture at 0 °C of $NaNO_2$ (1.38 g, 2×10^{-2} mol) in 60 mm of H_2O was slowly added to a cooled (0.02 mol) aryl amine derivatives and 50 mL of HCl, which was allowed to stir

https://doi.org/10.1021/acsomega.3c09072
ACS Omega 2024, 9, 18932−18945

in an ice bath for half an hour. The diazonium salt compound is always stored in the refrigerator, Scheme 1.

Scheme 1. Synthesis of (AZN) as the Azo Derivatives

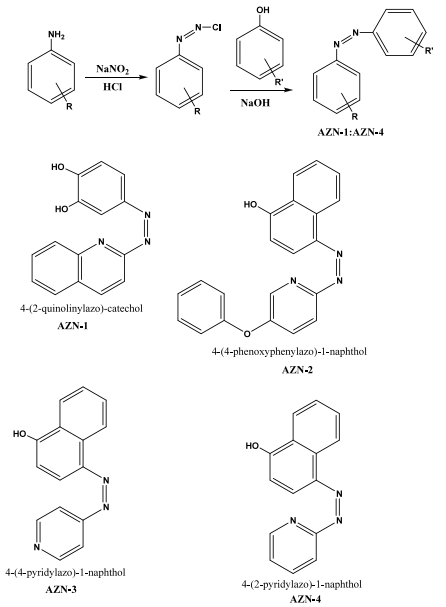

2.2.2. Step II: Coupling Process. The cooled compound of diazonium salt was slowly added to the cooled solution at 0 °C of phenol derivatives (0.02 mol) in sodium hydroxide (20% w/v) in an ice bath. Then, the azo dye will be formed. The final azo compound was formed via filtration of the crude precipitate, multiple cold-water washes, and crystallization from ethyl alcohol, Scheme 1.

*2.2.2.1. **4-(2-Quinolinylazo)- catechol (AZN-1)** (Figure S1).* Yellowish-red compound; yield (93%); mp. 144−145 °C; IR (cm^{-1}): 3292.98 (OH), 3015.47 (Ar−H), 16113.58 (C═N), 1587.95 (C═C); ^{1}H NMR (400 MHz, DMSO-d_6) δ (ppm):11.31(s, 1H, OH), 9.84 (s, 1H, OH), 8.38−8.00 (d, 1H, CHnaphthyl), 7.87−7.76 (m, 3H, (2CHnaphthyl + 1CHphenyl), 7.44−7.22(m, 3H, (1CHnaphthyl + 2CHphenyl)), 6.88−6.83 (m, 2H, CHnaphthyl); ^{13}C NMR (100 MHz, DMSO d6) δ (ppm): 178.20, 172.06, 157.14, 156.86, 140.61, 132.01, 131.65, 129.25, 129.10, 128.51, 127.88, 120.69, 119.84, 116.55; elemental analysis for $C_{14}H_{11}N_3O_2$ (calcd./fnd); C, 66.40/66.31; H, 4.40/4.33; N, 16.60/16.52.

*2.2.2.2. **4-(4-Phenoxyphenylazo)-1-naphthol (AZN-2)** (Figure S2).* Sunny-red product; yield (94%); mp. 193−194 °C; IR (cm^{-1}): 3283.07 (OH), 3052.52 (Ar−H), 1631.08 (C═N), 1600.78 (C═C); ^{1}H NMR (400 MHz, DMSO-d_6) δ (ppm): 8.53−8.51(d, 1H, CHphenyl), 8.18−8.16 (d, 1H, CHphenyl), 7.93−7.91(d, 1H, CHphenyl), 7.75−7.73 (d, 1H, CHphenyl), 7.62−7.58 (t, 2H, CHphenyl), 7.54−7.52(d, 1H, CHnaphthyl), 7.48−7.44 (t, 1H, CHphenyl), 7.44−7.38 (m, 5H, (4H(naphthyl + phenyl) + 1H (OH)), 7.38−7.36 (d, 2H, CH(naphthyl + phenyl)), 6.84−6.82 (d, 2H, 2Hnaphthyl); ^{13}C NMR (100 MHz, DMSO d6) δ (ppm): 172.10, 155.76, 145.30, 141.51, 135.49, 133.10, 131.01, 130.05, 128.39, 127.74, 126.42, 125.00, 123.07, 122.10, 117.22; elemental analysis for $C_{22}H_{16}N_2O_2$ (calcd./fnd); C, 77.65/77.41; H, 4.71/4.53; N, 8.24/8.13.

*2.2.2.3. **4-(4-Pyridylazo)-1-naphthol (AZN-3)** (Figure S3).* sunny-red compound; Yield (77%); mp. 181−183 °C; IR (cm^{-1}): 3421.10−3280.95 (OH), 3055.95 (Ar−H), 1615.25 (C═N), 1575.09 (C═C); ^{1}H NMR (400 MHz, DMSO-d_6) δ (ppm): 9.93 (s, br., 1H, HO−), 7.76−7.68 (m, 4H, CHpy), 7.38−7.14 (m, 6H, CHnaph.); ^{13}C NMR (100 MHz, DMSO d6) δ (ppm): 155.65, 145.23, 135.23, 135.03, 129.80, 128.19, 128.00, 126.63, 126.42, 123.16, 119.04, 109.12; elemental analysis for $C_{15}H_{11}N_3O$ (calcd./fnd); C, 77.29/77.17; H, 4.41/4.29; N, 16.87/16.81.

*2.2.2.4. **4-(2- Pyridylazo)-1-naphthol (AZN-4)** (Figure S4).* Sunny-red product; yield (85%); mp. 166−167 °C; IR (cm^{-1}): 3423−3285 (OH), 3050 (Ar−H), 1616.14 (C═N), 1587.13 (C═C); ^{1}H NMR (400 MHz, DMSO-d_6) δ (ppm): 7.77−7.74(m, 4H, CHpy), 7.40−7.36 (t, 2H, CHnaphth.), 7.27−7.26(d, 2H, CHnaphth.), 7.24−7.12(m, 2H, CHnaphth.); ^{13}C NMR (100 MHz, DMSO-d_6) δ (ppm):155.68, 135.06, 129.75, 128.22, 127.99, 126.59, 123.13, 119.65, 116.95, 109.14; elemental analysis for $C_{15}H_{11}N_3O$ (calcd./fnd); C, 77.29/77.11; H, 4.41/4.32; N, 16.87/16.71.

2.3. Electrochemical and Corrosion Inhibition Procedures. To conduct electrochemical tests, a carbon steel cylinder electrode is utilized as a working electrode, possessing an exposed surface area of 1 cm^2, and three different electrode configurations were employed. The reference electrode utilized an Ag/AgCl electrode saturated with KCl, while the counter electrode consisted of a 2 mm thick Pt wire. The corrosion cell contained 500 mL of a 3.5% sodium chloride solution. Afterward, carbon dioxide (under 0.9 bar pressure) was injected into the solution for one hour before immersing the working electrode. Following the initial hour, the pH of the solution was meticulously adjusted and maintained at a steady value of 4.25, allowing for a tolerance range of ±0.3. This indicated that the solution had achieved saturation concerning carbon dioxide. Throughout the experimental procedure, it is worth emphasizing that the introduction of carbon dioxide was consistently maintained to prevent any oxygen contamination. The electrochemical and corrosion inhibition processes were carried out using Gamry's potentiostat/galvanostat/ZRA framework. To stabilize the open-circuit potential (E_{OCP}), the carbon steel electrode was submerged in the corrosive solution for a duration of 40 min before conducting corrosion measurements. The potential dynamic polarization (PDP) tests were conducted at the specified temperature, with potentials ranging from −250 to +250 mV and a sweep rate of 0.2 mV s^{-1}. Electrochemical impedance spectroscopy (EIS) experiments were carried out at the E_{OCP}, using a 10 mV peak-to-peak voltage excitation within the frequency range of 100 kHz to 0.1 Hz. For consistency, each experiment was repeated three times to ensure reproducibility.

2.4. Surface Morphology Analysis Using the FE-SEM and FTIR Investigations. The carbon steel surface analysis was conducted using a FE-SEM Model JEOL (JSM 5410, Japan) after immersing the carbon steel specimen in a 3.5% NaCl solution saturated with CO_2 for 48 h before and after treating with 5×10^{-4} M of AZN-1 for 48 h at 50 °C. Furthermore, the protective film that developed on the carbon steel treated with 5×10^{-4} M of AZN-4 additive was investigated by collecting the produced layers after 48 h of immersion. This occurs by subjecting carbon steel samples to an abrasive process, subsequently rinsed with bidistilled water, and analyzed utilizing FTIR spectroscopy.

2.5. Computational Details. The Dmol^3 module of the BIOVIA Materials Studio 2017 software was employed to

https://doi.org/10.1021/acsomega.3c09072
ACS Omega 2024, 9, 18932−18945

perform density functional theory (DFT) calculations using a B_3LYP-functional and a DNP 4.4 basis set. These calculations aimed to minimize the energy of AZN molecules in a water environment.[37] Furthermore, the DFT calculations involved the utilization of the following equations to evaluate and calculate various properties such as E_{HOMO}, E_{LUMO}, energy gap (ΔE), electronegativity (χ), hardness (η), global softness (σ), number of electrons transferred (N), energy of back-donation ($E_{back\text{-}donation}$), and dipole moment (μ):[38]

$$\chi = \frac{-E_{HOMO} - E_{LUMO}}{2} \quad (1)$$

$$\eta = \frac{1}{\sigma} = \frac{E_{LUMO} - E_{HOMO}}{2} \quad (2)$$

$$\Delta N = \frac{\phi - \chi_{inh}}{2(\eta_{Fe} - \eta_{inh})} \quad (3)$$

$$\Delta E_{back\text{-}donation} = \frac{-\eta}{4} \quad (4)$$

In the equations, the symbol φ represents the work function of iron, while χ_{inh} denotes the electronegativity of the inhibitor. η_{Fe} and η_{inh} represent the chemical hardness of iron (0 eV) and the inhibitor, respectively.

In addition, the adsorption locator module in BIOVIA Materials Studio 2017 software was used to run MC simulations and determine the best possible arrangements for AZN molecules to adsorb onto the Fe (110) surface.[39] The COMPASS force field was used to achieve the best possible results for the adsorbate molecules.[40] Then, in a simulation box (37.24 Å × 37.24 Å × 59.81 Å), we discover the adsorption of AZN molecules, chloride ions, carbonate ions, hydronium ions, and water molecules onto the Fe (110) surface.[41] The selection of the Fe (110) surface for the adsorption simulation is predicated upon its identification as the predominant and most stable facet, accounting for more than 63% of the total surface area of iron crystals, as reported by prior studies.[42−45]

3. RESULTS AND DISCUSSION

3.1. PDP Measurements. The corrosion behavior of carbon steel in a CO_2-saturated 3.5% saline solution was investigated using the potentiodynamic polarization technique. Figure 1 shows the Tafel plots obtained from the experiments conducted under different conditions, including a blank solution and solutions containing AZN-4, AZN-3, AZN-2, and AZN-1. The corrosion rate as a function of the applied potential is visually depicted in the Tafel plots. These plots illustrate the anodic and cathodic polarization curves, which allow for determination of the corrosion potential and corrosion current density of the steel in each solution. By comparison of the results of these experiments, the effectiveness of the various AZN additives in inhibiting corrosion in the saline solution can be evaluated. The plots clearly show that the introduction of inhibitors into the blank solution had a noticeable effect on the polarized curves. A significant reduction in the rates of anodic and cathodic reactions was observed when comparing the curves of the blank and inhibitors (AZN-4, AZN-3, AZN-2, and AZN-1). However, the presence of the AZN inhibitors had a stronger influence on the anodic reactions than on the cathodic reactions. Although both types of reactions exhibited decreased corrosion, the inhibition of anodic and cathodic reactions,

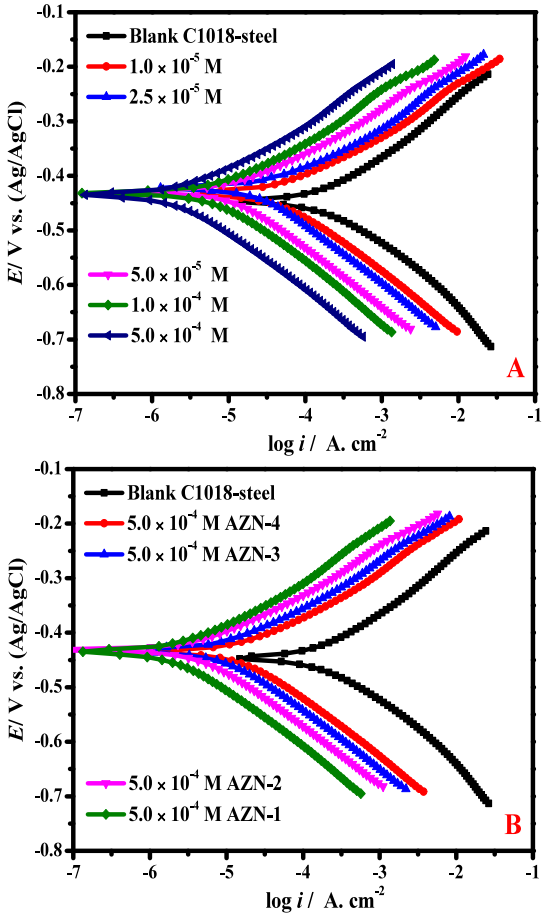

Figure 1. PDP diagrams for carbon steel in a CO_2-saturated 3.5% saline solution in the occurrence of diverse concentrations of AZN-1 (A) and 0.5 mmol/L of AZN compounds (B) at 50 °C.

which signify the dissolution of carbon steel, was more effective.[46] The Tafel polarization curves showed minimal changes in the Tafel slopes, suggesting that the presence of AZN-4, AZN-3, AZN-2, and AZN-1 did not alter the corrosion reaction pathway.

The obtained results from the Tafel plots, including the fitting and extrapolation of the log current versus potential curves to their intersections and the inhibition efficiency and surface coverage, are presented in Table 2. The data indicate that the Tafel constants (β_a and β_c) decrease when AZN compounds are added to the corrosion systems. This suggests that the AZN-4, AZN-3, AZN-2, and AZN-1 molecules contribute to both cathodic and anodic electrochemical reactions by adsorbing onto the metal surface and promoting its pristine condition.[47] Consequently, the addition of AZN-4, AZN-3, AZN-2, and AZN-1 molecules results in a significant reduction in the corrosion current (i_{cor}), with the lowest values obtained for AZN-1 (21.9 μAcm^{-2}), AZN-2 (36.2 μAcm^{-2}), AZN-3 (76.1 μAcm^{-2}), and AZN-4 (119.1 μAcm^{-2}) at 0.50 mM, as shown in Table 2. Similarly, the E_{cor} values shifted toward more positive or negative values in the presence of AZN-4, AZN-3, AZN-2, and AZN-1 molecules, with no clear direction observed. The difference between the E_{cor} values of the blank and inhibitor solutions ($\Delta E_{cor} = E_{cor}(blank) - E_{cor}(inhibitor)$) was generally less than ±85 mV in most cases, suggesting a mixed-type inhibition behavior of AZN-4, AZN-3, AZN-2, and AZN-1 molecules.[48]

https://doi.org/10.1021/acsomega.3c09072
ACS Omega 2024, 9, 18932−18945

Table 2. Corrosion Restrictions of Carbon Steel in a CO_2-Saturated 3.5% Saline Solution in the Occurrence of Diverse Concentrations of AZN Compounds at 50 °C

inhibitors code	C_i/mol L^{-1}	$i_{cor}/\mu A\ cm^{-2}$	E_{cor}/V (Ag/AgCl)	β_a/mV dec^{-1}	$-\beta_c$/mV dec^{-1}	θ	η_P/%
blank	0.0	1326.4 ± 56.4	−0.447	85.07	180.51	-	-
AZN-4	1.0×10^{-5}	1014.6 ± 46.5	−0.435	93.37	185.04	0.235	23.5
	2.5×10^{-5}	744.4 ± 35.4	−0.423	93.81	185.83	0.438	43.8
	5.0×10^{-5}	443.7 ± 20.1	−0.429	95.7	183.75	0.665	66.5
	1.0×10^{-4}	273.7 ± 9.6	−0.431	90.39	182.81	0.793	79.3
	5.0×10^{-4}	119.1 ± 4.8	−0.435	87.71	183.23	0.910	91.0
AZN-3	1.0×10^{-5}	966.5 ± 41.3	−0.425	95.79	188.06	0.271	27.1
	2.5×10^{-5}	695.9 ± 32.4	−0.441	91.69	189.25	0.475	47.5
	5.0×10^{-5}	367.1 ± 18.8	−0.436	95.15	185.12	0.723	72.3
	1.0×10^{-4}	195.9 ± 10.5	−0.428	99.43	193.31	0.852	85.2
	5.0×10^{-4}	76.1 ± 3.5	−0.534	96.57	186.58	0.942	94.2
AZN-2	1.0×10^{-5}	854.8 ± 37.1	−0.432	98.35	182.79	0.355	35.5
	2.5×10^{-5}	581.4 ± 27.2	−0.426	92.42	187.05	0.561	56.1
	5.0×10^{-5}	267.7 ± 15.7	−0.440	90.48	186.31	0.798	79.8
	1.0×10^{-4}	136.1 ± 8.3	−0.437	96.26	182.81	0.897	89.7
	5.0×10^{-4}	36.2 ± 2.1	−0.432	102.66	183.27	0.972	97.2
AZN-1	1.0×10^{-5}	797.6 ± 33.2	−0.422	93.98	182.62	0.398	39.8
	2.5×10^{-5}	544.9 ± 21.5	−0.434	94.28	185.35	0.589	58.9
	5.0×10^{-5}	229.9 ± 13.6	−0.445	96.54	187.04	0.826	82.6
	1.0×10^{-4}	113.4 ± 6.3	−0.428	88.96	183.68	0.914	91.4
	5.0×10^{-4}	21.9 ± 1.7	−0.337	101.83	185.89	0.983	98.3

The corrosion current value at a concentration of 0.01 mM was 1326.4 μAcm^{-2} for the blank 3.5% saline solution saturated with CO_2. For the AZN-4 compound, the corrosion current was 1014.6 $\mu A\ cm^{-2}$. The AZN-3 compound had a corrosion current of 966.5 μAcm^{-2}, while the AZN-2 compound had a corrosion current of 854.8 μAcm^{-2}. The AZN-1 compound had the lowest corrosion current at 797.6 μAcm^{-2}. These results suggest that the addition of AZN-4, AZN-3, AZN-2, and AZN-1 molecules reduces the level of corrosion of carbon steel. The current density gradually decreases with each successive addition of the inhibitor molecules. The values of β_a and β_c are also slightly affected by the presence of AZN-4, AZN-3, AZN-2, and AZN-1 molecules, providing evidence of their mixed inhibition performance through adsorption on both cathodic and anodic active sites.

The inhibition mechanisms of inhibitors can be categorized into (i) the geometry blocking postulated from the adsorption of inhibitor molecules, which is blocking the active sites of metal, (ii) the electrocatalytic impact endorsed either by the inhibitor molecules itself or its subsequent reaction products.[4950] From the analysis of the PDP curves, we can conclude that AZN compounds diminish the corrosive process predominantly through a geometry blocking approach, thereby occluding the active sites on the carbon steel substrate without participating directly in either the anodic or the cathodic reactions.

The protective capability (η_P/%) of AZN-4, AZN-3, AZN-2, and AZN-1 was intended from i_{cor} as per the following equation:[51]

$$\eta_P/\% = \left(\frac{i_{cor}^0 - i_{cor}^i}{i_{cor}^0}\right) \times 100 = \theta \times 100 \quad (5)$$

Where, i_{cor}^0= corrosion current density of the blank medium, i_{cor}^i= corrosion current density of any desired concentration of AZN-4, AZN-3, AZN-2, and AZN-1 molecules.

The protective abilities of AZN-4, AZN-3, AZN-2, and AZN-1 from the PDP measurements peaked at 91.02% (AZN-4), 94.26% (AZN-3), 97.27% (AZN-2), and 98.35% (AZN-1) at 0.5 mM, according to the data shown in Table 2. The corrosion protection of AZN-4, AZN-3, AZN-2, and AZN-1 molecules increased rapidly as more molecules were adsorbed, and the carbon steel surface became more coated. The adsorbed organic layers reduced the interaction between the corrosive medium and metallic surface, leading to enhanced adsorption and protection abilities. The presence of multiple hetero atoms (N) and donor−acceptor contacts from the aromatic conjugation systems to the empty d-shell of the carbon steel contributed to this boost in adsorption and protection. The presence of additional nitrogen atoms and OH in the molecular structure of AZN-1 may explain its higher inhibitory efficacy compared with the other compounds, as this allows for easier adsorption and improved protection.

3.2. EIS Measurements. In this study, electrochemical impedance spectroscopy (EIS) was employed to investigate the processes taking place on carbon steel substrates in systems with and without corrosion inhibitors. Furthermore, EIS was utilized to obtain crucial information on the resistance and capacitive behavior of the substrate, which helped in determining the specific inhibition process.[52]

The Nyquist profiles of carbon steel in a carbon dioxide-saturated sodium chloride solution were examined in Figure 2A,B. The profiles were obtained both without and with different concentrations of AZN molecules. The presence of AZN inhibitors enhanced the impedance behavior of carbon steel in the corrosive medium, as indicated by the Nyquist plot. The addition of higher concentrations of AZN resulted in larger semicircle diameters in the Nyquist profiles, indicating the formation of a protective layer between the base metal and the aggressive environments.[53] The Nyquist plots obtained do not exhibit perfectly circular shapes but instead show distorted loops (Figure 2A,B). These deviations are typically observed

https://doi.org/10.1021/acsomega.3c09072
ACS Omega 2024, 9, 18932−18945

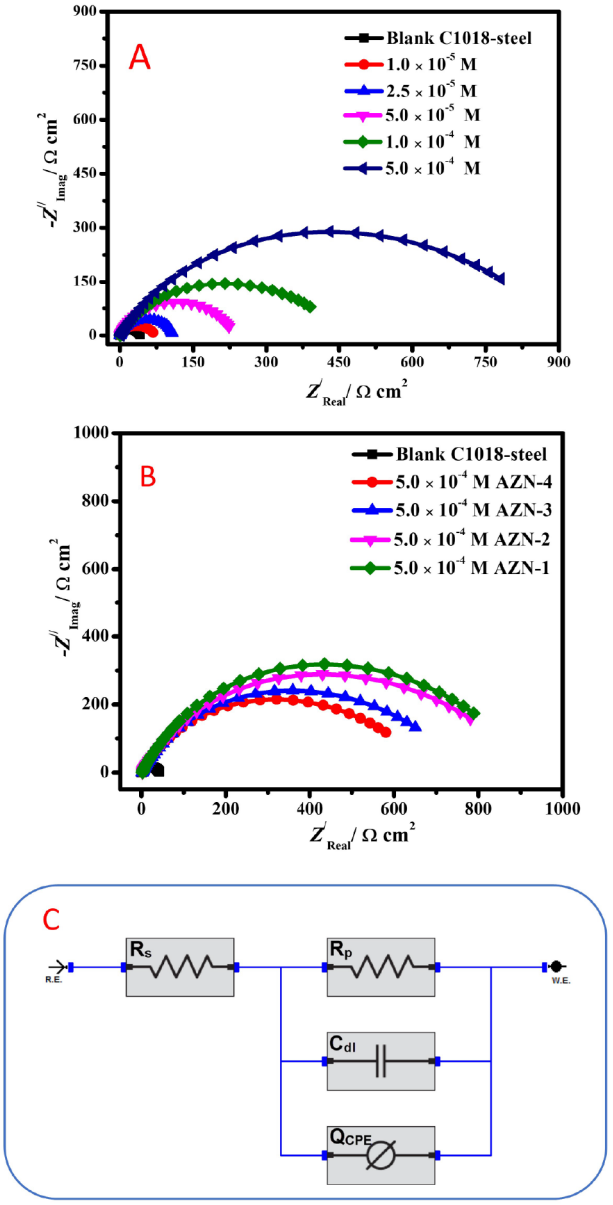

Figure 2. Nyquist diagrams for carbon steel in CO_2-saturated 3.5% saline solution in the occurrence of diverse concentrations of AZN-1 (A), 0.5 mmol/L of AZN compounds (B) at 50 °C, and (C) equivalent-circuit for the corrosion structures.

due to the unevenness and/or roughness of the surfaces of the carbon steel.[54]

To assess the electrochemical behavior of the carbon steel surface with and without an inhibitor, a suitable equivalent circuit was selected to model the experimental data. The comparison between the experimental data and the fitting results (Figure 2C) indicates a high level of accuracy. The circuit depicted in Figure 2C was employed in this investigation and comprises the solution resistance (R_s), polarization resistance (R_p), a constant phase element (CPE), and double-layer capacitance (C_{dl}). The justification for using R_p instead of the charge transfer resistance (R_{ct}) has been previously elucidated in detail.[55] The empirical outcomes were improved by categorizing them using a transference function and employing a CPE to achieve more precise modifications. The impedance of the CPE can be determined using equation:[56]

$$Z_{CPE} = \frac{1}{Q(i\omega)^n} = \frac{1}{Q(2i\pi f)^n} \quad (6)$$

The equation includes several variables: Q, representing the constant of CPE; i, representing the imaginary number; ω, representing the angular frequency in rad/s; f, representing the affected signal frequency; and n, indicating the phase shift. The phase shift is used to calculate surface maladjustment and the properties of Q. When $n = 1$, Q behaves as a pure capacitance, and when $n = 0$, Q can be considered a pure resistance. If $0 < n < 1$, Q is seen as a hybrid system.[57] The fitted circuit is used to estimate and record the impedance parameters, including R_s, R_p, C_{dl}, Y_0, and n, in Table 3. In blank solutions without inhibitors, the n value is 0.719, but it increases with the concentration of the inhibitors. Typically, a higher "n" value suggests a softer surface, while a lower value indicates a harder surface.[58] Therefore, it can be concluded that the presence of the surfactant compound led to a decrease in the surface roughness at the carbon steel interface. The low value of R_s suggests that the corrosive medium was stable, and the decreasing Y_0 value with increasing inhibitor dose indicates a significant reduction in charge accumulation at the carbon steel interface.

As shown in Table 3, the inclusion of the inhibitor in the corrosive solution led to an increase in R_p from 43.96 to 678.71, 805.26, 819.70, and 988.86 Ω cm^2 in the presence of 0.5 mM AZN-4, AZN-3, AZN-2, and AZN-1 molecules, respectively. Additionally, C_{dl} decreased from 516.81 to 36.08, 7.46, 14.90, and 10.51 μF cm^{-2} for the same molecules, respectively. The R_p values consistently increased with higher concentrations of the inhibitor. A higher R_p value indicates an increase in the diameter of the Nyquist semicircle as well as an increase in the magnitude of the absolute impedance. These findings suggest that the addition of inhibitors significantly enhances the corrosion inhibition of carbon steel in a CO_2-saturated 3.5% NaCl solution. According to the Helmholtz model, the C_{dl} value can be attributed to the thickness of the electrical double film, which acts as a protective layer following the equation:[59]

$$C_{dl} = \varepsilon\varepsilon_0 A/\delta \quad (7)$$

In this study, we took into account factors such as the dielectric constant (ε), thickness of the double layer (δ), vacuum permittivity (ε_0), and electrode interface area (A). The findings indicated that as the inhibitor concentration increased, the value of C_{dl} decreased. This can be explained by the increase in the double layer thickness and/or the decrease in the local dielectric constant.[60] As a result, the surface coverage increased due to the successful adsorption of surfactant species, resulting in improved protection capabilities.

The protective ability (η_E/%) of AZN-4, AZN-3, AZN-2, and AZN-1 was intended from R_p as per the following eq 8:

$$\eta_E/\% = \left(\frac{R_p^i - R_p^0}{R_p^i}\right) \times 100 = \theta \times 100 \quad (8)$$

where R_p^0= polarization resistance of the blank medium, R_p^i = polarization resistance of any desired concentration of AZN-4, AZN-3, AZN-2, and AZN-1 molecules. The η_E/value increases with the concentration of [AZN], reaching 93.5%,

https://doi.org/10.1021/acsomega.3c09072
ACS Omega 2024, 9, 18932−18945

Table 3. EIS Restrictions and Protection Proficiency for Carbon Steel in a CO_2-Saturated 3.5% Saline Solution in the Occurrence of Diverse Concentrations of AZN Compounds at 50 °C

					Q_{CPE}			
inhibitor codes	$C_{inh.}$/mol/L	R_s/Ω cm^2	R_p/Ω cm^2± SD	C_{dl}/F cm^{-2}× 10^{-6}	$Y_0/\mu\Omega^{-1}$ s^n cm^{-2}	n	θ	η_E/%
blank	0	0.90	43.96 ± 3.5	516.81	109.20	0.719	-	-
AZN-4	1.0 × 10^{-5}	0.97	54.98 ± 4.1	207.69	68.67	0.795	0.200	20.0
	2.5 × 10^{-5}	1.99	82.11 ± 6.3	167.86	48.74	0.817	0.464	46.5
	5.0 × 10^{-5}	1.54	159.83 ± 12.7	94.05	35.88	0.859	0.724	72.5
	1.0 × 10^{-4}	1.58	363.22 ± 21.5	40.34	15.11	0.837	0.878	87.9
	5.0 × 10^{-4}	1.70	678.71 ± 42.9	36.08	6.06	0.859	0.935	93.5
AZN-3	1.0 × 10^{-5}	1.89	71.51 ± 5.8	102.26	33.58	0.805	0.385	38.5
	2.5 × 10^{-5}	2.00	100.37 ± 8.4	91.99	24.01	0.858	0.561	56.2
	5.0 × 10^{-5}	2.50	202.44 ± 13.3	55.57	19.32	0.827	0.782	78.3
	1.0 × 10^{-4}	2.25	375.82 ± 24.8	10.35	6.45	0.896	0.883	88.3
	5.0 × 10^{-4}	3.43	805.26 ± 50.8	7.46	1.74	0.832	0.945	94.5
AZN-2	1.0 × 10^{-5}	0.98	67.22 ± 5.4	164.95	52.40	0.804	0.345	34.6
	2.5 × 10^{-5}	1.14	103.22 ± 7.6	136.20	37.60	0.823	0.574	57.4
	5.0 × 10^{-5}	1.38	214.81 ± 15.2	85.13	28.31	0.853	0.795	79.5
	1.0 × 10^{-4}	1.52	443.60 ± 27.1	21.58	10.85	0.861	0.900	90.1
	5.0 × 10^{-4}	1.96	819.70 ± 60.6	14.90	4.77	0.889	0.946	94.6
AZN-1	1.0 × 10^{-5}	1.62	77.31 ± 6.2	117.56	37.66	0.807	0.431	43.1
	2.5 × 10^{-5}	1.89	112.39 ± 9.1	97.09	27.07	0.912	0.608	60.9
	5.0 × 10^{-5}	2.16	247.98 ± 16.7	60.67	20.34	0.870	0.822	82.3
	1.0 × 10^{-4}	2.39	482.55 ± 30.5	15.45	7.47	0.844	0.908	90.9
	5.0 × 10^{-4}	3.17	988.86 ± 75.6	10.51	2.76	0.915	0.950	95.6

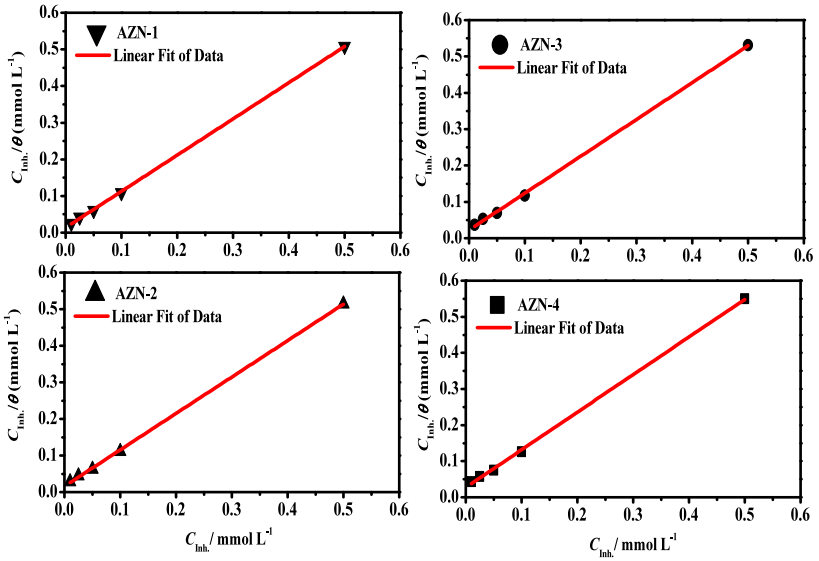

Figure 3. Langmuir adsorption plots for AZN compounds for C-steel in a CO_2-saturated 3.5% saline solution at 50 °C using PDP data.

94.5%, 94.6%, and 95.6% for the AZN-4, AZN-3, AZN-2, and AZN-1 molecules, respectively, at the optimal dosage of 0.5 mM.

3.3. Adsorption Isotherm. The molecules AZN-4, AZN-3, AZN-2, and AZN-1, which were studied, consist of heteroatoms, aromatic rings, and azo groups that have the ability to adhere to the surface of the steel and create a protective layer.[61]

The following adsorption mechanisms[62] can be utilized to generate these layers: (i) physical adsorption occurs due to electrostatic interactions between protonated organic molecules and the charged metal surface; (ii) chemical adsorption arises from the formation of coordination bonds between the substrate's vacant d orbital and the heteroatoms' lone electron pair; or (iii) adsorption results from a combination of both types. Each adsorption isotherm graph was individually examined to determine and analyze the most effective adsorption isotherm (such as Langmuir, Flory−Huggins, Temkin, Frumkin, Freundlich, and Kinetic models) for the tested AZN compounds.

The correlation coefficients (R^2) obtained from regression analysis of the Langmuir model[63] indicated a strong agreement between the adsorption behavior of AZN-4, AZN-3, AZN-2, and AZN-1 on the surface of carbon steel and the Langmuir isotherm equation represented as[64]

$$\frac{C_{inh.}}{\theta} = \frac{1}{K_{ads}} + C_{inh.} \quad (9)$$

https://doi.org/10.1021/acsomega.3c09072
ACS Omega 2024, 9, 18932−18945

Table 4. Langmuir Adsorption Parameters for AZN Compounds for C-Steel in a CO_2-Saturated 3.5% Saline Solution at 50 °C using PDP Outcomes

inhibitors code	R^2	S = slope	intercept	K_{ads}/L mol^{-1}	ΔG^{o}_{ads}/kJ mol^{-1}
AZN-1	0.99989	0.988	1.38×10^{-5}	7.2×10^{4}	−40.82
AZN-2	0.99987	0.995	1.59×10^{-5}	6.3×10^{4}	−40.46
AZN-3	0.99971	1.012	2.24×10^{-5}	4.4×10^{4}	−39.51
AZN-4	0.99974	1.041	2.73×10^{-5}	3.6×10^{4}	−38.96

where the equilibrium constant for the adsorption−desorption processes on the metal substrate is denoted as K_{ads}, the molarity of the tested inhibitors represented by C_{inh}, and the calculated θ obtained from PDP techniques. In Figure 3, a straight fitting line with a slope and correlation coefficient close to 1 can be observed for the graph of C_{inh} plotted against C_{inh}/θ. The equation used to quantify K_{ads} was derived from the standard free energy of adsorption (ΔG^{o}_{ads}):[65]

$$\Delta G^{o}_{ads} = -RT \ln K_{ads} C_{water} \quad (10)$$

where R stands for the universal gas constant, T stands for the absolute temperature, and C_{water} represents the amount of water in the solution by molarity. The thermodynamics of the investigated compounds (AZN-4, AZN-3, AZN-2, and AZN-1) being adsorbed are shown in Table 4. Assuming that the tested compounds (AZN-4, AZN-3, AZN-2, and AZN-1) adsorb spontaneously on the surface of the carbon steel due to the ΔG^{o}_{ads} values being negative. A stronger adsorption property and therefore better inhibitory property are also indicated by higher K_{ads} values.[66] Generally speaking, ΔG^{o}_{ads} with absolute values of (20 kJ mol^{-1}) or less is the result of electrostatic contact or physisorption. Comparable ΔG^{o}_{ads} values (between 20 and 40 kJ mol^{-1}) imply charge sharing and bond formation, but values around 40 kJ mol^{-1} or higher negative values indicate these processes.[67] This demonstrates the physical and chemical adsorption of AZN-4, AZN-3, AZN-2, and AZN-1 on the surface of C-steel, with chemical adsorption having a particularly potent adsorption impact.[68] Table 4 also showed that AZN-2 and AZN-1 molecules had higher K_{ads} values than did AZN-3 and AZN-4, which can be read as the inhibition of AZN-4, AZN-3, AZN-2, and AZN-1.

3.4. Surface Morphology Analysis. *3.4.1. FE-SEM Analysis.* SEM analysis was performed to examine the effect of a specific concentration of the AZN-1 molecule on the surface morphology of carbon steel. The steel was immersed in a CO_2-saturated 3.5% saline solution with or without the addition of 0.5 mmol/L of AZN-1 at 50 °C for 48 h and then evaluated. In the absence of any inhibitor, corrosion significantly deteriorated the surface of the carbon steel in the CO_2-saturated saline solution (Figure 4A). However, after the use of inhibitors, the carbon steel surface was found to be smooth and free of pits (Figure 4B). This suggests that the inhibitors formed a protective coating on the carbon steel surface. Chemical and electrochemical techniques were used to assess the effectiveness of the inhibitors in providing protection.

3.4.2. FTIR Analysis. FTIR inspection has emerged as a significant technique for determining the bonding type of organic inhibitors present at the steel/solution interface.[69] The FTIR instrument has been extensively employed to analyze protective layers created on the surface of steel. FTIR analysis of the pristine AZN-4 inhibitor is displayed in Figure 5-line A.

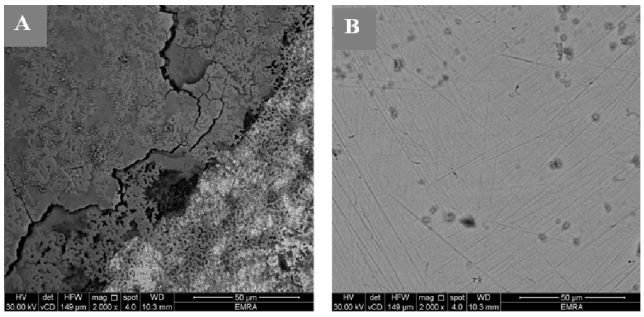

Figure 4. SEM of carbon steel in (A) CO_2-saturated 3.5% saline solution and (B) containing 0.5 mmol/L of AZN-1 after immersion for 48 h. at 50 °C.

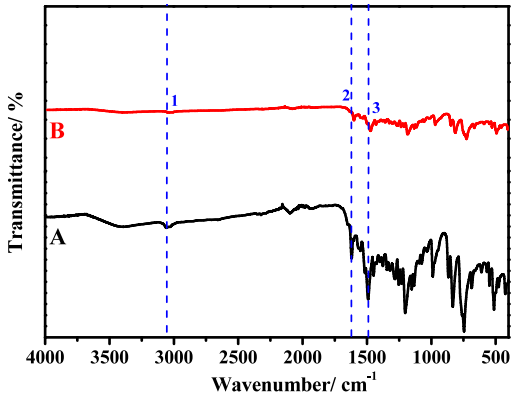

Figure 5. FTIR spectra of (A) crude AZN-4, (B) adsorbed film formed on the carbon steel surface after exposure to CO_2-saturated 3.5% NaCl solution containing 5×10^{-4} M of AZN-4 for 48 h at 50 °C.

Figure 5, line B shows the FTIR analysis results of the protective layer formed on the carbon steel surface following exposure to a 3.5% NaCl solution saturated with CO_2, which also contained 5×10^{-4} M of AZN-4. In the case of the adsorbed film (line B), it is evident that the −OH stretching at 3063 cm^{-1} (peak **1**) has disappeared. This indicates that the oxygen atom in the OH group forms a coordination bond with Fe^{2+} on the steel surface, leading to the formation of a Fe^{2+}−AZN-4 complex at the anodic centers of the steel interface. The C═N stretching frequency has shifted from 1631 to 1608 cm^{-1} (peak **2**), while the C═C bond frequency has changed from 1509 to 1490 cm^{-1} (peak **3**). Based on these observations from the FTIR analysis, it can be concluded that the protective layer consists of a [Fe−AZN-4] complex.[70]

3.5. Computational Calculations (DFT). Figure 6 illustrates the distributions of the lowest unoccupied molecular orbital (LUMO) and the highest occupied molecular orbital (HOMO), along with the optimal structures of the AZN compounds. The corresponding computational parameters can be found in Table 5. According to the Frontiers molecular

https://doi.org/10.1021/acsomega.3c09072
ACS Omega 2024, 9, 18932−18945

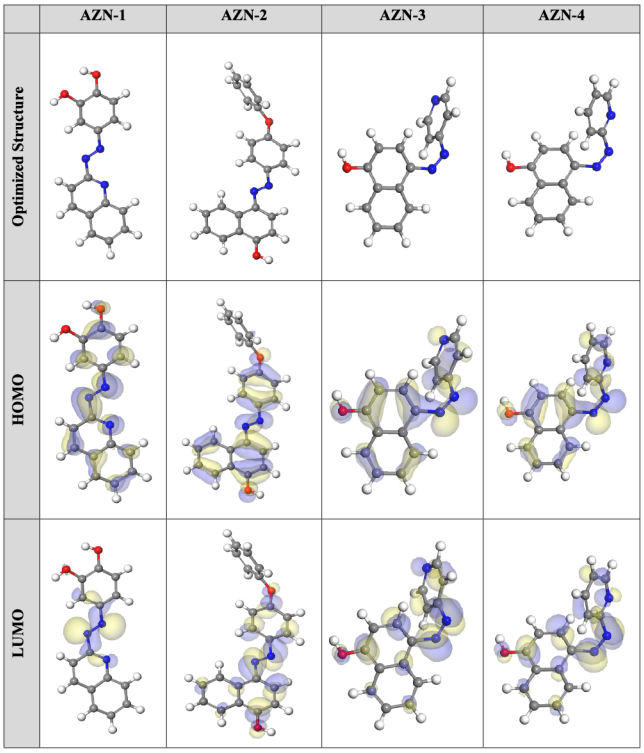

Figure 6. Optimized structure and HOMO and LUMO orbitals for the examined **AZN** molecules using the Dmol^3 module.

Table 5. Parameters of DFT of the AZN Molecules using the Dmol^3 module

parameters	AZN-1	AZN-2	AZN-3	AZN-4
E_{HOMO} (eV)	−4.72	−4.79	−4.88	−4.82
E_{LUMO} (eV)	−3.60	−3.07	−2.82	−3.04
$\Delta E = E_{LUMO} - E_{HOMO}$ (eV)	1.12	1.72	2.06	1.78
electronegativity (χ)	4.16	3.93	3.85	3.93
global hardness (η)	0.56	0.86	1.03	0.89
global softness (σ)	1.78	1.16	0.97	1.12
the number of electrons transferred (ΔN)	2.54	1.78	1.53	1.72
$\Delta E_{back\text{-}donation}$	−0.14	−0.22	−0.26	−0.22
dipole moments (μ) Debye	8.44	5.98	4.60	5.12

orbital theory (FMO) concept, the LUMO and HOMO energies of an inhibitor determine its capacity for donor or acceptor interaction.[71] Hence, a desirable corrosion inhibitor molecule should have a low energy level of the lowest unoccupied molecular orbital (E_{LUMO}) and a high energy level of the highest occupied molecular orbital (E_{HOMO}). In comparison to the AZN-2, AZN-3, and AZN-4 molecules (with E_{HOMO} values of −4.79, −4.88, and −4.82 eV, respectively), the AZN-1 molecule has the highest E_{HOMO} value (−4.72 eV), as shown in Table 5. Figure 6 illustrates that the HOMO levels of the additive molecules are situated on the phenyloxy, diazenyl, 4-pyridinyl, 2-pyridinyl, naphthanyl-1-ol, and quinolinyl groups, which are ideal for electrophilic attacks on the carbon steel surface. This supports the effectiveness of the inhibitor molecule in adsorbing onto the steel surface and thereby enhancing inhibition efficiency, which aligns with the empirical findings. Conversely, AZN-1 has a lower E_{LUMO} value (−3.60 eV) compared to AZN-2, AZN-3, and AZN-4 (−3.07, −2.82, 3.04 eV, respectively) as shown in Table 5, confirming the heightened protective capability of the AZN-1 molecule, consistent with previous research.

Similarly, the energy gap (ΔE) plays a crucial role in determining the efficacy of an inhibitor molecule in inhibiting corrosion.[72] The effectiveness of the inhibitor molecule increases as the ΔE value decreases. As shown in Table 5, the AZN-1 molecule has a lower E value (1.12 eV) compared to the AZN-2, AZN-3, and AZN-4 molecules (1.72, 2.06, and 1.78 eV, respectively), indicating a higher likelihood of absorption on the C1018-Steel surface.

Inhibitors often display low electronegativity values, indicating a capability for electron donations to metal surface.[73] However, if the inhibitor molecule's electronegativity (χ) value is high, it is capable of accepting the electron from the atoms on the metal surface. It is tracking via back-donation, resulting in a more stable covalent bond between the inhibitor and metal surface.[74] From Table 5, we can infer that the molecules of AZN compounds have a somewhat high electronegativity, allowing them to back-donate electrons and form a more stable connection with the carbon steel surface.

Similarly, the molecular softness (σ) and hardness (η) can be employed to evaluate the molecule's activity and durability; soft molecules are more effective corrosion inhibitors because they can more easily transfer electrons to the metal surface by adsorption.[75] Table 5 shows that the AZN-1 molecule has a greater σ value and smaller η value than the AZN-2, AZN-3, and AZN-4 molecules, reflecting a more relaxed dedication of electrons to the carbon steel substrate and superior inhibitory properties.

Additionally, the electron transfer fraction and $E_{back\text{-}donation}$ determine the ability of the inhibitor to donate or accept electrons. Consequently, if the ΔN is positive, there is a higher likelihood of electron transfer between the inhibitor molecule and the metal interface atoms. Conversely, if ΔN is negative, electron transfer between the metal atoms and the inhibitor molecule (i.e., back-donation) is feasible.[76] Table 5 shows that all of the ΔN values for the examined AZN molecules are positive, indicating their capability to donate electrons to the surface of carbon steel. Moreover, when $\eta > 0$, the $E_{back\text{-}donation}$ becomes negative, suggesting that electrons are being withdrawn from the molecule and return back through a back-donation pathway, which is preferred in terms of dynamics.[77] The negative values of $E_{back\text{-}donation}$ for the AZN compounds in Table 5 indicate that they can form strong bonds with the carbon steel surface through back-donation.[78]

In the corrosion inhibition prediction mechanism, the dipole moment is also a significant factor.[79] A higher dipole moment enhances the molecule's ability to adsorb onto the metal surface and increases its distortion energy, resulting in improved corrosion suppression.[80] According to Table 5, the AZN-1 molecules have a higher dipole moment value (8.44 debye) compared to that of the AZN-2, AZN-3, and AZN-4 molecules (5.98, 4.60, and 5.12 debye, respectively). This indicates that the AZN-1 molecules have a greater tendency to be adsorbed onto the carbon steel interface, thereby strengthening the protection.

Additionally, the Dmol^3 module incorporates molecular electrostatic potential mapping (MEP), which can identify the active sites of inhibitor molecules. MEP is a three-dimensional visualization tool used to illustrate the net electrostatic significance distributed across a molecule based on its overall charge distribution.[81] Figure 7 displays MEP maps, where the color red signifies the area with the greatest electron density

https://doi.org/10.1021/acsomega.3c09072
ACS Omega 2024, 9, 18932−18945

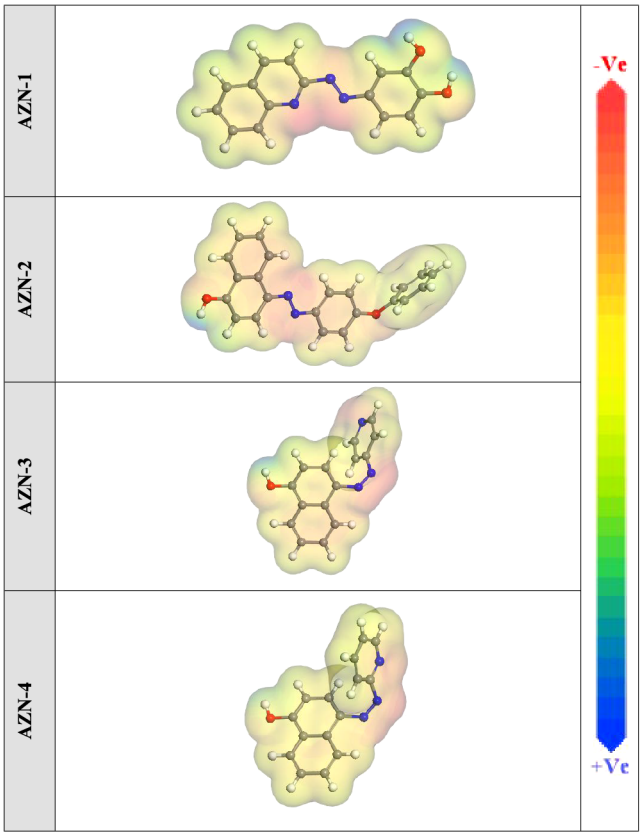

Figure 7. Graphical attendance of the MEP of the AZN molecules utilizing the Dmol3 module.

and, consequently, the most negative charge (indicating a nucleophilic reaction), while the color blue represents the region with the highest positive charge (indicating an electrophilic reaction).[82] From Figure 7, it can be observed that the electron density is lowest above the benzene rings, while the most negative contributions are mainly located above the nitrogen and oxygen atoms. The regions with higher electron density (indicated by red zones) correspond to areas where the inhibitor species have strong interactions with the carbon steel surface and can form stable, adsorbed protective layers.

3.6. MC Simulations. In order to understand the adsorption process and the attraction between the inhibitor species and the carbon steel surface, Monte Carlo simulations were conducted. Figure 8 shows the adsorption location module, which illustrates the optimal adsorption configurations of AZN compound molecules on the carbon steel surface in an acidic solution. This indicates an enhancement in adsorption and the highest surface coverage.[83] The results of Monte Carlo simulations, shown in Table 6, were used to determine the adsorption energies, which are of great importance. It was observed that the AZN-1 molecule had a higher negative adsorption energy value (−8277.71 kcal mol^{-1}) compared to the AZN-2, AZN-3, and AZN-4 molecules (−8216.72, 8182.71, and −8130.60 kcal mol^{-1}, respectively). This indicates that the AZN-1 molecule strongly adsorbs onto the surface of C1018-Steel, forming a stable adsorbed film.[84] The adsorption energy values for the AZN-1 molecule, both before and after geometry optimization, are lower compared with the AZN-2, AZN-3, and AZN-4 molecules (Table 6). Specifically, the unrelaxed value is −5911.03 kcal mol^{-1}, and the relaxed value is −2366.68 kcal mol^{-1}. This indicates that AZN-1 offers a greater level of protection compared with the other molecules.

The energy of the metal/adsorbates arrangement can be determined by analyzing the dE_{ads}/dN_i values, provided that the adsorbed inhibitor molecule or other adsorbates molecules are excluded.[39,85] According to the data presented in Table 6, the AZN-1 molecule has a higher dE_{ads}/dN_i value (−408.84 kcal mol^{-1}) compared to AZN-2, AZN-3, and AZN-4 molecules (−387.57, −371.30, and 351.66 kcal mol^{-1}, respectively). This indicates that AZN-1 has better adsorption capabilities than do the other molecules. Additionally, the dE_{ads}/dN_i values for water, hydronium, carbonate, and chloride ions are approximately −18.39, −94.18, −154.65, and 135.33 kcal mol^{-1}, respectively. The low values for these species compared to AZN molecules suggest that the adsorption of AZN molecules is superior to those of water, hydronium, carbonate, and chloride ions. Theoretical and experimental evidence support the idea that AZN molecules form a strong adsorbed protective layer on the surface of carbon steel, providing corrosion resistance in a corrosive environment.

4. CONCLUSIONS

Based on the findings of this study, four azo derivatives (AZN-1, AZN-2, AZN-3, and AZN-4) were successfully synthesized and characterized using spectroscopic techniques. The corrosion protection abilities of these compounds were then evaluated in a corrosive environment (carbon dioxide-saturated sodium chloride solution) through various methods, including electrochemical impedance spectroscopy, Tafel polarization, field emission-scanning electron microscopy with energy-dispersive X-ray spectroscopy, density functional theory calculations, and Monte Carlo simulations. The results demonstrated that AZN-1, AZN-2, AZN-3, and AZN-4 inhibitors effectively prevented the corrosion of carbon steel under mild conditions. Notably, AZN-1 exhibited the highest level of protection, with a 98.3% inhibition efficiency at a concentration of 0.5 mM, as determined by Tafel polarization measurements. The addition of these inhibitors in the corrosive environment further enhanced corrosion protection. The values of R_p (polarization resistance) increased from 43.96 to 678.71, 805.26, 819.70, and 988.86 Ω cm^2, while the values of C_{dl} (double-layer capacitance) decreased from 516.81 to 36.08, 7.46, 14.90, and 10.51 μF cm^{-2} in the presence of 0.5 mM AZN-4, AZN-3, AZN-2, and AZN-1 molecules, respectively. The inhibitors acted as mixed-type additives with both physical and chemical adsorption occurring at the interface between the carbon steel and the AZN compounds. The Langmuir isotherm model was found to accurately describe the adsorption of the AZN compounds, as evidenced by the calculated values of K_{ads}. The FE-SEM and FTIR analyses confirmed that adsorption played a primary role in the corrosion protection mechanism. Furthermore, the use of density functional theory calculations has elucidated the active sites of the AZN molecules. In addition, Monte Carlo simulations have revealed both the adsorption configurations and the corresponding energies for the AZN molecules on the Fe (110) surface and also corroborated the superior inhibitory efficacy of AZN-1 consistent with the empirical findings. This may be attributed to the enhanced capability of AZN-1 for electron contribution, resulting from the presence of two hydroxy groups ortho to each other, which signifies a robust electron-donating propensity. Besides, the presence of a

https://doi.org/10.1021/acsomega.3c09072
ACS Omega 2024, 9, 18932−18945

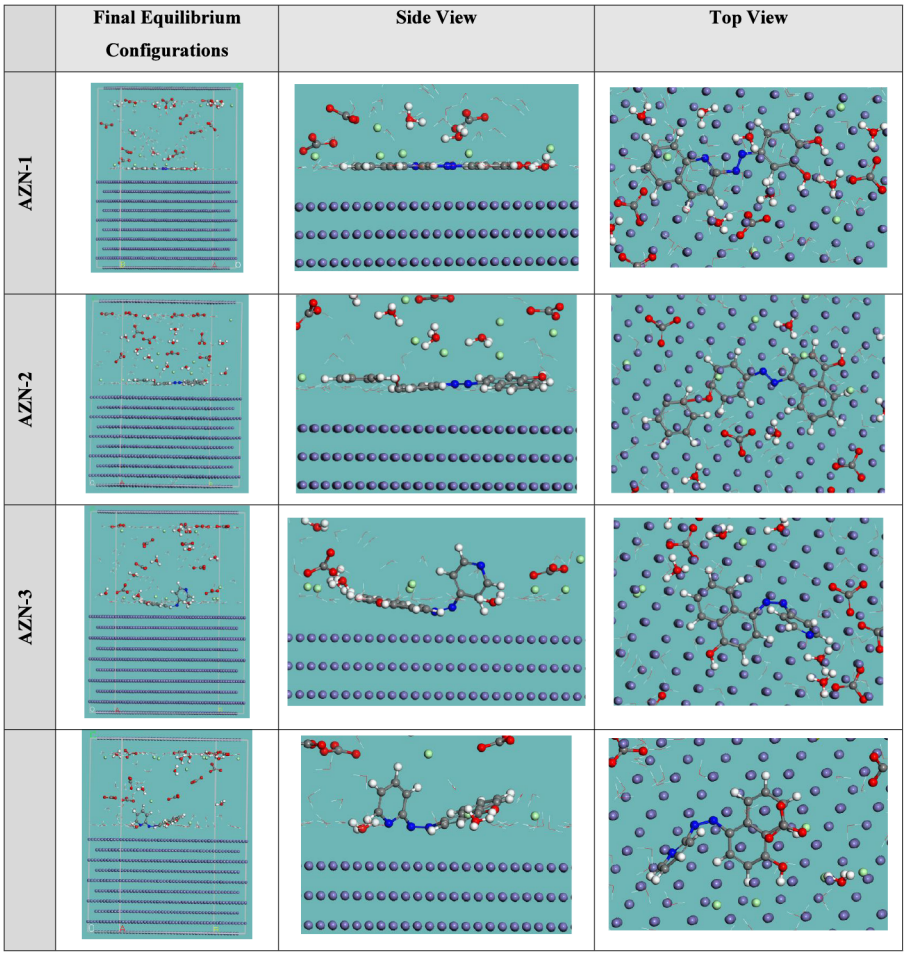

Figure 8. Potential adsorption configurations for the AZN compounds molecules on Fe (110) substrate accomplished by the adsorption locator module.

Table 6. Data Computed by the MC Simulations for the Adsorption of the AZN Molecules on Fe (110)

corrosion systems	adsorption energy/ kcal mol^{-1}	rigid adsorption energy/ kcal mol^{-1}	deformation energy/ kcal mol^{-1}	dE_{ads}/dN_i: inhibitor kcal mol^{-1}	dE_{ads}/dN_i: Cl^- ions kcal mol^{-1}	dE_{ads}/dN_i: CO_3^{2-} ions kcal mol^{-1}	dE_{ads}/dN_i: H_3O^+ ions kcal mol^{-1}	dE_{ads}/dN_i: water kcal mol^{-1}
Fe (110)/**AZN-1**/corrosive media	−8277.71	−5911.03	−2366.68	−408.84	−134.83	−155.83	−90.53	−18.73
Fe (110)/**AZN-2**/corrosive media	−8216.72	−5873.61	−2343.11	−387.57	−137.65	−155.86	−91.09	−18.38
Fe (110)/**AZN-3**/corrosive media	−8182.71	−5856.50	−2326.20	−371.30	−136.42	−153.94	−99.11	−18.12
Fe (110)/**AZN-4**/corrosive media	−8130.60	−5815.92	−2314.68	−351.66	−132.41	−152.95	−95.97	−18.33

nitrogen atom within the quinoline structure, which cannot participate in the resonance, results in the localization of electron lone pairs on the nitrogen atom; this allows for easier adsorption and improved protection. Conversely, AZN-2 is characterized by the presence of a single hydroxyl group and an oxygen atom positioned between two benzene rings; this configuration facilitates the oxygen participation in the resonance and leads to the delocalization of electron lone pairs, thereby diminishing the electron density. Along similar lines, the compounds AZN-3 and AZN-4, although comprising a single hydroxyl group, exhibit a diminished electron-donating capacity when compared with AZN-1. In conclusion, this comprehensive study presents effective and environmentally friendly inhibitors that have potential applications in corrosion prevention under mild conditions. Additionally, long-term exposure tests under realistic sweet conditions, including varying temperatures, flow rates, and corrosive species, can provide insights into the durability and effectiveness of the inhibitors over extended periods.

■ ASSOCIATED CONTENT

Supporting Information

The Supporting Information is available free of charge at https://pubs.acs.org/doi/10.1021/acsomega.3c09072.

Characterization data of the synthesized azo derivatives; ^{1}H NMR and ^{13}C NMR spectra for AZN-1; FTIR, ^{1}H NMR and ^{13}C NMR spectra for AZN-2; FTIR, ^{1}H

https://doi.org/10.1021/acsomega.3c09072
ACS Omega 2024, 9, 18932−18945

NMR, and ^{13}C NMR spectra for AZN-3; ^{1}H NMR and ^{13}C NMR spectra for AZN-4 (PDF)

AUTHOR INFORMATION

Corresponding Author

Kamal Shalabi − *Department of Chemistry, College of Science and Humanities in Al-Kharj, Prince Sattam Bin Abdulaziz University, Al-Kharj 11942, Saudi Arabia; Chemistry Department, Faculty of Science, Mansoura University, Mansoura 35516, Egypt;* orcid.org/0000-0001-5478-6369; Email: k.shalabi@psau.edu.sa

Authors

Hany M. Abd El-Lateef − *Department of Chemistry, College of Science, King Faisal University, Al-Ahsa 31982, Saudi Arabia; Chemistry Department, Faculty of Science, Sohag University, Sohag 82524, Egypt*

Mohamed M. Hammouda − *Department of Chemistry, College of Science and Humanities in Al-Kharj, Prince Sattam Bin Abdulaziz University, Al-Kharj 11942, Saudi Arabia; Chemistry Department, Faculty of Science, Mansoura University, Mansoura 35516, Egypt*

Antar A. Abdelhamid − *Chemistry Department, Faculty of Science, Sohag University, Sohag 82524, Egypt; Chemistry Department, Faculty of Science, Al-Baha University, Al-Baha 1988, Saudi Arabia*

Complete contact information is available at: https://pubs.acs.org/10.1021/acsomega.3c09072

Author Contributions

K.S. contributed to conceptualization, supervision, investigation, methodology, resources, formal analysis, data curation, funding acquisition, writing − original draft, and writing − review and editing. H.M.A.E.-L. contributed to conceptualization, supervision, investigation, methodology, resources, formal analysis, data curation, writing − original draft, and writing − review and editing. M.M.H. contributed to conceptualization, supervision, investigation, methodology, resources, formal analysis, data curation, funding acquisition, writing − original draft, and writing − review and editing. A.A.A. contributed to conceptualization, supervision, investigation, methodology, resources, formal analysis, data curation, funding acquisition, writing − original draft, and writing − review and editing.

Notes

The authors declare no competing financial interest.

ACKNOWLEDGMENTS

The authors extend their appreciation to the Deputyship for Research & Innovation, Ministry of Education in Saudi Arabia for funding this research work through the project number (IF2/PSAU/2022/01/22252).

REFERENCES

(1) Umoren, S. A.; Ekanem, U. F. Inhibition of Mild Steel Corrosion in H2SO4 using Exudate Gum Frompachylobus Edulisand Synergistic Potassium Halide Additives. *Chem. Eng. Commun.* **2010**, *197* (10), 1339−1356.

(2) Awad, M. I. Eco friendly corrosion inhibitors: Inhibitive action of quinine for corrosion of low carbon steel in 1 m HCl. *J. Appl. Electrochem.* **2006**, *36* (10), 1163−1168.

(3) Kahyarian, A.; Singer, M.; Nesic, S. Modeling of uniform CO2 corrosion of mild steel in gas transportation systems: A review. *J. Nat. Gas Sci. Eng.* **2016**, *29*, 530−549.

(4) Ontiveros-Rosales, M.; Espinoza-Vázquez, A.; Rodríguez Gómez, F. J.; Valdez-Rodríguez, S.; Miralrio, A.; Acosta-Garcia, B. A.; Castro, M. Imidazolate of 1-butyl-3-ethyl imidazole as corrosion inhibitor on API 5L X52 steel in NaCl saturated with CO2. *J. Mol. Liq.* **2022**, *363*, 119826−119826.

(5) Chauhan, D. S.; Quraishi, M. A.; Sorour, A. A.; Verma, C. A review on corrosion inhibitors for high-pressure supercritical CO2 environment: Challenges and opportunities. *J. Pet. Sci. Eng.* **2022**, *215*, 110695−110695.

(6) Jiang, H.; Wang, B.; Liu, J.; Zhou, J.; Liu, C. Corrosion inhibition of Q235 and X65 steels in CO2-saturated solution by 2-phenyl imidazoline. *Arabian J. Chem.* **2023**, *16* (6), 104774.

(7) Onyeachu, I. B.; Quraishi, M. A.; Obot, I. B. A synthesized pyrimidine derivative with highly efficient long-term corrosion protection for API X60 steel in CO2-saturated NACE brine ID196 under hydrodynamic condition. *J. Mol. Struct.* **2023**, *1284*, 135399.

(8) Zhang, Q. H.; Hou, B. S.; Zhang, G. A. Inhibitive and adsorption behavior of thiadiazole derivatives on carbon steel corrosion in CO2-saturated oilfield produced water: Effect of substituent group on efficiency. *J. Colloid Interface Sci.* **2020**, *572*, 91−106.

(9) Hu, J.; Xiong, Q.; Chen, L.; Zhang, C.; Zheng, Z.; Geng, S.; Yang, Z.; Zhong, X. Corrosion inhibitor in CO2-O2-containing environment: Inhibition effect and mechanisms of Bis(2-ehylhexyl) phosphate for the corrosion of carbon steel. *Corros. Sci.* **2021**, *179*, 109173.

(10) Chen, X.; Cui, W.; Liu, C.; Yang, J.; Wang, B.; Wang, X. Synergism of alkylbenzene sulfonate and cetyltrimethylammonium bromide on corrosion inhibition of carbon steel in CO2 -saturated solutions. *Colloids Surf., A* **2023**, *658*, 130735.

(11) Usman, B. J.; Ali, S. A. Carbon Dioxide Corrosion Inhibitors: A review. *Arabian J. Sci. Eng.* **2018**, *43* (1), 1−22.

(12) Singh, A.; Lin, Y.; Ebenso, E. E.; Liu, W.; Pan, J.; Huang, B. Gingko biloba fruit extract as an eco-friendly corrosion inhibitor for J55 steel in CO2 saturated 3.5% NaCl solution. *J. Ind. Eng. Chem.* **2015**, *24*, 219−228.

(13) Raja, P. B.; Sethuraman, M. G. Natural products as corrosion inhibitor for metals in corrosive media - A review. *Mater. Lett.* **2008**, *62* (1), 113−116.

(14) Wang, D.-Y.; Wang, J.-H.; Li, H.-J.; Wu, Y.-C. Pectin-amino acid derivatives as highly efficient green inhibitors for the corrosion of N80 steel in CO2-saturated formation water. *Ind. Crops Prod.* **2022**, *189*, 115866.

(15) Singh, A.; Ansari, K. R.; Quraishi, M. A. Inhibition effect of natural polysaccharide composite on hydrogen evolution and P110 steel corrosion in 3.5 wt% NaCl solution saturated with CO2: Combination of experimental and surface analysis. *Int. J. Hydrogen Energy* **2020**, *45* (46), 25398−25408.

(16) Wang, X.; Guo, H.; Cai, S.; Xu, X. Expired antihypertensive drugs as eco-friendly and efficient corrosion inhibitors for carbon steel in CO2-saturated oilfield water: Experimental and theoretical approaches. *J. Mol. Struct.* **2023**, *1294*, 136555.

(17) Benkhaya, S.; M' Rabet, S.; El Harfi, A. A review on classifications, recent synthesis and applications of textile dyes. *Inorg. Chem. Commun.* **2020**, *115*, 107891.

(18) Benkhaya, S.; M'Rabet, S.; El Harfi, A. Classifications, properties, recent synthesis and applications of azo dyes. *Heliyon* **2020**, *6* (1), No. e03271−e03271.

(19) Wagner-Wysiecka, E.; Szarmach, M.; Chojnacki, J.; Łukasik, N.; Luboch, E. Cation sensing by diphenyl-azobenzocrowns. *J. Photochem. Photobiol., A* **2017**, *333*, 220−232.

(20) Yusoff, M. H.; Azmi, M. N.; Hussin, M. H.; Osman, H.; Raja, P. B.; Rahim, A. A.; Awang, K. An Electrochemical Evaluation of Synthesized Coumarin-Azo Dyes as Potential Corrosion Inhibitors for Mild Steel in 1 M HCl Medium. *Int. J. Electrochem. Sci.* **2020**, *15* (12), 11742−11756.

(21) Gürses, A.; Açıkyıldız, M.; Güneş, K.; Gürses, M. S. Classification of Dye and Pigments. In *In Springer Briefs in Molecular Science*; Springer International Publishing, 2016; pp. 31−45.

(22) Zhao, R.; Tan, C.; Xie, Y.; Gao, C.; Liu, H.; Jiang, Y. One step synthesis of azo compounds from nitroaromatics and anilines. *Tetrahedron Lett.* **2011**, *52* (29), 3805−3809.
(23) Leriche, G.; Budin, G.; Brino, L.; Wagner, A. Optimization of the Azobenzene Scaffold for Reductive Cleavage by Dithionite; Development of an Azobenzene Cleavable Linker for Proteomic Applications. *Eur. J. Org. Chem.* **2010**, *2010* (23), 4360−4364.
(24) Ravi, B. N.; Keshavayya, J.; Mallikarjuna, N. M.; Kumar, V.; Kandgal, S. Synthesis, characterization and pharmacological evaluation of 2-aminothiazole incorporated azo dyes. *J. Mol. Struct.* **2020**, *1204*, 127493.
(25) Favre-Besse, F.-C.; Poirel, O.; Bersot, T.; Kim-Grellier, E.; Daumas, S.; El Mestikawy, S.; Acher, F. C.; Pietrancosta, N. Design, synthesis and biological evaluation of small-azo-dyes as potent Vesicular Glutamate Transporters inhibitors. *Eur. J. Med. Chem.* **2014**, *78*, 236−247.
(26) Fouda, A. S.; Mukhtar, M. M. New arylazodyes as corrosion inhibitors for mild steel in HCL solution. *Chem. Eng. Commun.* **2011**, *198* (9), 1111−1128.
(27) Obaid, H. T.; Kadhum, M. Y.; Abdulnabi, A. S. Azo Schiff base derived from 2-hydroxy-1-naphthaldehyde as corrosion inhibitors for carbon steel in HCl medium: Experimental and theoretical studies. *Mater. Today: Proc.* **2022**, *60*, 1394−1401.
(28) Elaryian, H. M.; Bedair, M. A.; Bedair, A. H.; Aboushahba, R. M.; Fouda, A. E.-A. S. Synthesis, characterization of novel coumarin dyes as corrosion inhibitors for mild steel in acidic environment: Experimental, theoretical, and biological studies. *J. Mol. Liq.* **2022**, *346*, 118310.
(29) El-Tabei, A. S.; El-Tabey, A. E.; El Basiony, N. M. Newly imine-azo dicationic amphiphilic for corrosion and sulfate-reducing bacteria inhibition in petroleum processes: Laboratory and theoretical studies. *Appl. Surf. Sci.* **2022**, *573*, 151531.
(30) A Altalhi, A. Anticorrosion Investigation of New Diazene-Based Schiff Base Derivatives as Safe Corrosion Inhibitors for API X65 Steel Pipelines in Acidic Oilfield Formation Water: Synthesis, Experimental, and Computational Studies. *ACS Omega* **2023**, *8* (34), 31271−31280.
(31) Zobeidi, A.; Neghmouche Nacer, S.; Atia, S.; Kribaa, L.; Kerassa, A.; Kamarchou, A.; AlNoaimi, M.; Ghernaout, D.; Ali, M. A.; Lagum, A. A.; et al.et al. Corrosion Inhibition of Azo Compounds Derived from Schiff Bases on Mild Steel (XC70) in (HCl, 1 M DMSO) Medium: An Experimental and Theoretical Study. *ACS Omega* **2023**, *8* (24), 21571−21584.
(32) Youssif, M. M.; El-Nahass, M. N.; Fayed, T. A.; El-Daly, H. A.; El-Gamil, M. M.; Eldesoky, A. M. Tunable Anticorrosive Effects of Newly Synthesized Benzothiazole Azo Dyes by Potassium Iodide Synergism for Carbon Steel in 1 M HCl: Combined Experimental and Theoretical Studies. *ACS Omega* **2023**, *8* (31), 28314−28332.
(33) Abdou, M. M.; Younis, O.; El-Katori, E. E. Synthesis, experimental and theoretical studies of two aryl-azo derivatives clubbed with 2-acetylphenol and their application as novel luminescent coatings with high anticorrosion efficiency. *J. Mol. Liq.* **2022**, *360*, 119506.
(34) Abbas, M. A.; Eid, A. M.; Abdou, M. M.; Elgendy, A.; El-Saeed, R. A.; Zaki, E. G. Multifunctional Aspects of the Synthesized Pyrazoline Derivatives for AP1 5L X60 Steel Protection Against MIC and Acidization: Electrochemical, In Silico, and SRB Insights. *ACS Omega* **2021**, *6* (13), 8894−8907.
(35) Abdulridha, A. A.; Albo Hay Allah, M. A.; Makki, S. Q.; Sert, Y.; Salman, H. E.; Balakit, A. A. Corrosion inhibition of carbon steel in 1 M H2SO4 using new Azo Schiff compound: Electrochemical, gravimetric, adsorption, surface and DFT studies. *J. Mol. Liq.* **2020**, *315*, 113690.
(36) Al-Saidi, H. M.; Gouda, G. A.; Abdel-Hakim, M.; Alsenani, N. I.; Alfarsi, A.; Mahross, M. H.; Farghaly, O. A.; Hosny, S. Synthesis and Characterization of Ni(II), Cu(II), Zn(II) and Azo Dye Based on 1,10-o-Phenanthroline Binary Complexes: Corrosion Inhibition Properties and Computational Studies. *Int. J. Electrochem. Sci.* **2022**, *17* (3), 220333.
(37) Abd El-Lateef, H. M.; Sayed, A. R.; Shalabi, K. Synthesis and theoretical studies of novel conjugated polyazomethines and their application as efficient inhibitors for C1018 steel pickling corrosion behavior. *Surf. Interfaces* **2021**, *23*, 101037.
(38) El-Lateef, H. M. A.; Abdallah, Z. A.; Ahmed, M. S. M. Solvent-free synthesis and corrosion inhibition performance of Ethyl 2-(1,2,3,6-tetrahydro-6-oxo-2-thioxopyrimidin-4-yl)ethanoate on carbon steel in pickling acids: Experimental, quantum chemical and Monte Carlo simulation studies. *J. Mol. Liq.* **2019**, *296*, 111800.
(39) Dehghani, A.; Mostafatabar, A. H.; Bahlakeh, G.; Ramezanzadeh, B. A detailed study on the synergistic corrosion inhibition impact of the Quercetin molecules and trivalent europium salt on mild steel; electrochemical/surface studies, DFT modeling, and MC/MD computer simulation. *J. Mol. Liq.* **2020**, *316*, 113914.
(40) Feng, Y.; Chen, S.; Guo, W.; Zhang, Y.; Liu, G. Inhibition of iron corrosion by 5,10,15,20-tetraphenylporphyrin and 5,10,15,20-tetra-(4-chlorophenyl)porphyrin adlayers in 0.5M H2SO4 solutions. *J. Electroanal. Chem.* **2007**, *602* (1), 115−122.
(41) Abd-Elaal, A. A.; Elbasiony, N. M.; Shaban, S. M.; Zaki, E. G. Studying the corrosion inhibition of some prepared nonionic surfactants based on 3-(4-hydroxyphenyl) propanoic acid and estimating the influence of silver nanoparticles on the surface parameters. *J. Mol. Liq.* **2018**, *249*, 304−317.
(42) Guo, L.; Ren, X.; Zhou, Y.; Xu, S.; Gong, Y.; Zhang, S. Theoretical evaluation of the corrosion inhibition performance of 1,3-thiazole and its amino derivatives. *Arabian J. Chem.* **2017**, *10* (1), 121−130.
(43) Guo, L.; Obot, I. B.; Zheng, X.; Shen, X.; Qiang, Y.; Kaya, S.; Kaya, C. Theoretical insight into an empirical rule about organic corrosion inhibitors containing nitrogen, oxygen, and sulfur atoms. *Appl. Surf. Sci.* **2017**, *406*, 301−306.
(44) Arya, A.; Carter, E. A. Structure, bonding, and adhesion at the TiC(100)/Fe(110) interface from first principles. *J. Chem. Phys.* **2003**, *118* (19), 8982−8996.
(45) Xu, L.; Kirvassilis, D.; Bai, Y.; Mavrikakis, M. Atomic and molecular adsorption on Fe(110). *Surf. Sci.* **2018**, *667*, 54−65.
(46) Batah, A.; Anejjar, A.; Bammou, L.; Belkhaouda, M.; Salghi, R.; Bazzi, L. Carbon steel corrosion inhibition by rind and leaves extracts of grapefruit in 1.0 M hydrochloric acid. *J. Mater. Environ. Sci.* **2017**, *8* (9), 3070−3080.
(47) Bentiss, F.; Lebrini, M.; Vezin, H.; Chai, F.; Traisnel, M.; Lagrenè, M. Enhanced corrosion resistance of carbon steel in normal sulfuric acid medium by some macrocyclic polyether compounds containing a 1,3,4-thiadiazole moiety: AC impedance and computational studies. *Corros. Sci.* **2009**, *51* (9), 2165−2173.
(48) Singh, A.; Ansari, K. R.; Quraishi, M. A.; Kaya, S. Theoretically and experimentally exploring the corrosion inhibition of N80 steel by pyrazol derivatives in simulated acidizing environment. *J. Mol. Struct.* **2020**, *1206*, 127685−127685.
(49) Okafor, P. C.; Zheng, Y. Synergistic inhibition behaviour of methylbenzyl quaternary imidazoline derivative and iodide ions on mild steel in H2SO4 solutions. *Corros. Sci.* **2009**, *51* (4), 850−859.
(50) Heydari, M.; Javidi, M. Corrosion inhibition and adsorption behaviour of an amido-imidazoline derivative on API 5L X52 steel in CO2-saturated solution and synergistic effect of iodide ions. *Corros. Sci.* **2012**, *61*, 148−155.
(51) El-Hajjaji, F.; Ech-Chihbi, E.; Rezki, N.; Benhiba, F.; Taleb, M.; Chauhan, D. S.; Quraishi, M. A.; et al. Electrochemical and theoretical insights on the adsorption and corrosion inhibition of novel pyridinium-derived ionic liquids for mild steel in 1 M HCl. *J. Mol. Liq.* **2020**, *314*, 113737−113737.
(52) Saha, S. K.; Murmu, M.; Murmu, N. C.; Banerjee, P. Evaluating electronic structure of quinazolinone and pyrimidinone molecules for its corrosion inhibition effectiveness on target specific mild steel in the acidic medium: A combined DFT and MD simulation study. *J. Mol. Liq.* **2016**, *224*, 629−638.
(53) Singh, A.; Ansari, K. R.; Chauhan, D. S.; Quraishi, M. A.; Lgaz, H.; Chung, I.-M. Comprehensive investigation of steel corrosion inhibition at macro/micro level by ecofriendly green corrosion

https://doi.org/10.1021/acsomega.3c09072
ACS Omega 2024, 9, 18932−18945

inhibitor in 15% HCl medium. *J. Colloid Interface Sci.* **2020**, *560*, 225−236.
(54) Ansari, K. R.; Quraishi, M. A. Experimental and computational studies of naphthyridine derivatives as corrosion inhibitor for N80 steel in 15% hydrochloric acid. *Phys. E (Amsterdam, Neth.)* **2015**, *69*, 322−331.
(55) Singh, A.; Ansari, K. R.; Quraishi, M. A.; Lgaz, H.; Lin, Y. Synthesis and investigation of pyran derivatives as acidizing corrosion inhibitors for N80 steel in hydrochloric acid: Theoretical and experimental approaches. *J. Alloys Compd.* **2018**, *762*, 347−362.
(56) Ansari, K. R.; Quraishi, M. A.; Singh, A. Schiff's base of pyridyl substituted triazoles as new and effective corrosion inhibitors for mild steel in hydrochloric acid solution. *Corros. Sci.* **2014**, *79*, 5−15.
(57) Haque, J.; Ansari, K. R.; Srivastava, V.; Quraishi, M. A.; Obot, I. B. Pyrimidine derivatives as novel acidizing corrosion inhibitors for N80 steel useful for petroleum industry: A combined experimental and theoretical approach. *J. Ind. Eng. Chem.* **2017**, *49*, 176−188.
(58) Bentiss, F.; Lebrini, M.; Lagrenèe, M. Thermodynamic characterization of metal dissolution and inhibitor adsorption processes in mild steel/2,5-bis(n-thienyl)-1,3,4-thiadiazoles/hydrochloric acid system. *Corros. Sci.* **2005**, *47* (12), 2915−2931.
(59) Soltani, N.; Salavati, H.; Rasouli, N.; Paziresh, M.; Moghadasi, A. Adsorption and Corrosion Inhibition Effect of Schiff Base Ligands on Low Carbon Steel Corrosion in Hydrochloric Acid Solution. *Chem. Eng. Commun.* **2016**, *203* (6), 840−854.
(60) Kowsari, E.; Payami, M.; Amini, R.; Ramezanzadeh, B.; Javanbakht, M. Task-specific ionic liquid as a new green inhibitor of mild steel corrosion. *Appl. Surf. Sci.* **2014**, *289*, 478−486.
(61) Yilmaz, N.; Fitoz, A.; Ergun, Ÿ.; Emregül, K. C. A combined electrochemical and theoretical study into the effect of 2-((thiazole-2-ylimino)methyl)phenol as a corrosion inhibitor for mild steel in a highly acidic environment. *Corros. Sci.* **2016**, *111*, 110−120.
(62) Gonzalez-Rodriguez, J. G.; Zeferino-Rodriguez, T.; Ortega, D. M.; Serna, S.; Campillo, B.; Casales, M.; Valenzuela, E.; Juárez-Islas, J. A. Effect of microestructure on the CO2 corrosion inhibition by carboxyamidoimidazolines on a pipeline steel. *Int. J. Electrochem. Sci.* **2007**, *2* (11), 883−896.
(63) Musa, A. Y.; Kadhum, A. A. H.; Mohamad, A. B.; Takriff, M. S. Molecular dynamics and quantum chemical calculation studies on 4,4-dimethyl-3-thiosemicarbazide as corrosion inhibitor in 2.5 M H 2SO4. *Mater. Chem. Phys.* **2011**, *129* (1−2), 660−665.
(64) Desimone, M. P.; Grundmeier, G.; Gordillo, G.; Simison, S. N. Amphiphilic amido-amine as an effective corrosion inhibitor for mild steel exposed to CO2 saturated solution: Polarization, EIS and PM-IRRAS studies. *Electrochim. Acta* **2011**, *56* (8), 2990−2998.
(65) Migahed, M. A.; Elgendy, A.; El-Rabiei, M. M.; Nady, H.; Zaki, E. G. Novel Gemini cationic surfactants as anti-corrosion for X-65 steel dissolution in oilfield produced water under sweet conditions: Combined experimental and computational investigations. *J. Mol. Struct.* **2018**, *1159*, 10−22.
(66) Faisal, M.; Saeed, A.; Shahzad, D.; Abbas, N.; Ali Larik, F.; Ali Channar, P.; Abdul Fattah, T.; Muhammad Khan, D.; Aaliya Shehzadi, S. General properties and comparison of the corrosion inhibition efficiencies of the triazole derivatives for mild steel. *Corros. Rev.* **2018**, *36* (6), 507−545.
(67) Singh, A.; Ansari, K. R.; Lin, Y.; Quraishi, M. A.; Lgaz, H.; Chung, I.-M.-M. Corrosion inhibition performance of imidazolidine derivatives for J55 pipeline steel in acidic oilfield formation water: Electrochemical, surface and theoretical studies. *J. Taiwan Inst. Chem. Eng.* **2019**, *95*, 341−356.
(68) Sun, Z.; Singh, A.; Xu, X.; Chen, S.; Liu, W.; Lin, Y. Inhibition effect of pomelo peel extract for N80 steel in 3.5% NaCl saturated with CO2 solution. *Res. Chem. Intermed.* **2017**, *43* (11), 6719−6736.
(69) Lalitha, A.; Ramesh, S.; Rajeswari, S. Surface protection of copper in acid medium by azoles and surfactants. *Electrochim. Acta* **2005**, *51* (1), 47−55.
(70) Silverstein, R. M.; Webster, F. X.; Kiemle, D. *Spectrometric Identification of Organic Compounds*, 7th ed. ed.; Wiley, 2005.
(71) Zhang, D.; Xing, P.; Pan, R.; Lin, X.; Sha, M.; Jiang, B. Preparation and Surface Properties Study of Novel Fluorine-Containing Methacrylate Polymers for Coating. *Materials* **2018**, *11* (11), 2258.
(72) Abd El-Lateef, H. M.; Shalabi, K.; Tantawy, A. H. Corrosion inhibition and adsorption features of novel bioactive cationic surfactants bearing benzenesulphonamide on C1018-steel under sweet conditions: Combined modeling and experimental approaches. *J. Mol. Liq.* **2020**, *320*, 114564.
(73) Palaniappan, N.; Cole, I. S.; Kuznetsov, A. E. Experimental and computational studies of graphene oxide covalently functionalized by octylamine: electrochemical stability, hydrogen evolution, and corrosion inhibition of the AZ13 Mg alloy in 3.5% NaCl. *RSC Adv.* **2020**, *10* (19), 11426−11434.
(74) Lukovits, I.; Kálmán, E.; Zucchi, F. Corrosion Inhibitors—Correlation between Electronic Structure and Efficiency. *Corrosion* **2001**, *57* (1), 3−8.
(75) Yesudass, S.; Olasunkanmi, L. O.; Bahadur, I.; Kabanda, M. M.; Obot, I. B.; Ebenso, E. E. Experimental and theoretical studies on some selected ionic liquids with different cations/anions as corrosion inhibitors for mild steel in acidic medium. *J. Taiwan Inst. Chem. Eng.* **2016**, *64*, 252−268.
(76) Debab, H.; Douadi, T.; Daoud, D.; Issaadi, S.; Chafaa, S. Electrochemical and Quantum Chemical Studies of Adsorption and Corrosion Inhibition of Two New Schiff Bases on Carbon Steel in Hydrochloric Acid Media. *Int. J. Electrochem. Sci.* **2018**, *13* (7), 6958−6977.
(77) Gao, G.; Liang, C. Electrochemical and DFT studies of β-amino-alcohols as corrosion inhibitors for brass. *Electrochim. Acta* **2007**, *52* (13), 4554−4559.
(78) Dichiarante, V.; Milani, R.; Metrangolo, P. Natural surfactants towards a more sustainable fluorine chemistry. *Green Chem.* **2018**, *20* (1), 13−27.
(79) Abd El-Lateef, H. M.; Shalabi, K.; Tantawy, A. H. Corrosion inhibition of carbon steel in hydrochloric acid solution using newly synthesized urea-based cationic fluorosurfactants: experimental and computational investigations. *New J. Chem.* **2020**, *44* (41), 17791−17814.
(80) Goyal, M.; Vashist, H.; Kumar, S.; Bahadur, I.; Benhiba, F.; Zarrouk, A. Acid corrosion inhibition of ferrous and non-ferrous metal by nature friendly Ethoxycarbonylmethyltriphenylphosphonium Bromide (ECMTPB): Experimental and MD simulation evaluation. *J. Mol. Liq.* **2020**, *315*, 113705.
(81) Oyebamiji, A. K.; Adeleke, B. B. Quantum chemical studies on inhibition activities of 2,3-dihydroxypropyl-sulfanyl derivative on carbon steel in acidic media. *Int. J. Corros. Scale Inhib.* **2018**, *7* (4), 498−508.
(82) Gece, G.; Bilgiç, S. Quantum chemical study of some cyclic nitrogen compounds as corrosion inhibitors of steel in NaCl media. *Corros. Sci.* **2009**, *51* (8), 1876−1878.
(83) Madkour, L. H.; Kaya, S.; Obot, I. B. Computational, Monte Carlo simulation and experimental studies of some arylazotriazoles (AATR) and their copper complexes in corrosion inhibition process. *J. Mol. Liq.* **2018**, *260*, 351−374.
(84) Shalabi, K.; Helmy, A. M.; El-Askalany, A. H.; Shahba, M. M. New pyridinium bromide mono-cationic surfactant as corrosion inhibitor for carbon steel during chemical cleaning: Experimental and theoretical studies. *J. Mol. Liq.* **2019**, *293*, 111480.
(85) Özcan, M.; Dehri, İ.; Erbil, M. Organic sulphur-containing compounds as corrosion inhibitors for mild steel in acidic media: correlation between inhibition efficiency and chemical structure. *Appl. Surf. Sci.* **2004**, *236* (1−4), 155−164.

https://doi.org/10.1021/acsomega.3c09072
ACS Omega 2024, 9, 18932−18945